Investigation of Passive Control Devices for Potential Application to a Launch Vehicle Structure to Reduce the Interior Noise Levels During Launch

14th February 2001

Preliminary Report for Stage 2

Prepared For: AFOSR

Contract Number: F6256299M9179

Prepared by: Professor Colin H. Hansen
Dr. Anthony C. Zander
Dr. Ben S. Cazzolato
Mr Rick C. Morgans
Department of Mechanical Engineering
The University of Adelaide SA 5005
AUSTRALIA
14th February 2001

Contents

1 Introduction

The worked discussed in the following report is an extension of the work undertaken by Dr Steve Griffin of the Air Force Research Lab at Kirtland AFB, New Mexico during his participation in the AFOSR Windows on Science program at the University of Adelaide, South Australia in 1998. The previous work involved an investigation of the application of active feedback control of the launch vehicle structural vibration using radiation mode vibration levels as the cost function to minimise interior noise levels. The small benefit of active control, compared to the passive effect of the un-excited actuators attached to the structure, has been the impetus behind the work conducted here which is directed at optimising the passive effect of vibration reduction devices.

1.1 Stage 1

The work presented in the following report continues the work reported in the stage 1 study[1] where the optimal configuration of a passive Vibro-Acoustic Device (VAD) mounted to the interior of a small cylinder was investigated. The VAD consisted of an acoustic absorber and a vibration absorber (Tuned Mass Damper, TMD) in the one device. This is realised in practice using a loudspeaker, which has an enclosed rear side and its front side exposed. The loudspeaker diaphragm and backing cavity act as an acoustic tuned absorber, while attaching the entire device to the structure using spring connectors provides the vibration absorber device. The system used for stage 1 was a 2.142m long, 6.35mm thick steel cylinder with an outside diameter of 0.514m. One end was capped with a rigid plywood end-cap and the other had a flexible aluminium panel with a thickness of 3.376mm. The VAD was attached to the aluminium panel. Figure 1 shows photographs of the experimental setup of the exterior of the small cylinder and the VAD attached to the panel.

(a) Steel cylinder (b) Vibro-acoustic device

Figure 1: Photographs of Experimental Setup.

In the previous study a numerical framework was developed for determining the response of a coupled vibro-acoustic system using a combination of Modal Coupling Analysis and Finite Element Analysis that enabled the response of the structure and internal cavities to be determined. Boundary Element Analysis provided the solutions for the external pressure field and Finite Element Analysis provided the structural and cavity resonant frequencies and mode shapes. The

models were coupled using the modal coupling technique, which coupled the *in-vacuo* modal model of the structure to the rigid-walled modal model of the cavity.

A variety of passive devices were investigated, and it was found that it was very difficult to use a VAD as a reactive device to control sound pressure over a broad bandwidth. The effect of the VADs that were analysed was to reduce the amplitude of the in-phase panel/VAD modes by mass loading the panel modes. However, the VAD also introduced an out-of-phase mode that boosted the sound transmission at high frequencies. In between the resonance frequencies of the two lowest order panel/VAD modes, a strong anti-resonance existed, which resulted from the uncoupled VAD mode and did provide some reduction in sound transmission into the cavity.

The optimal VAD design used the TMD as a highly reactive device with an uncoupled resonance frequency just below the upper bound of the frequency band of interest. The optimal loudspeaker diaphragm configuration was highly lossy so that it reduced the modal amplitude of a single acoustic mode. Local flexure of the cylinder end cap to which the VAD was attached reduced the effectiveness of the VAD's and alternative attachment techniques were investigated to reduce such flexure. Figure 2 shows FEA results of the out-of-phase panel/VAD modes for three different spring attachments.

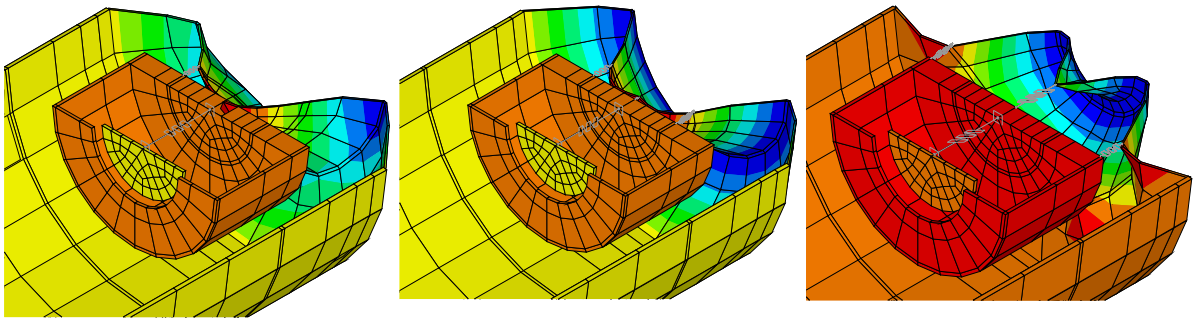

(a) 3 Spring, original attachment diameter

(b) 7 Spring, original attachment diameter

(c) 7 Spring, larger attachment diameter

Figure 2: Finite element model showing the mode shapes of the out-of-phase mode for the 3 different spring configurations.

It should be noted that in almost all the cases considered, the equivalent mass (achieved by simply smearing the VAD mass over the flexible panel), provided optimal passive control over a larger bandwidth. This is not surprising, since the VAD introduces another higher order mode that boosts high frequency transmission over that achieved by the empty structure. The only benefit of the VAD (apart from the mass loading of the primary structural mode) is the anti-resonance generated (at the uncoupled VAD natural frequency).

1.2 Stage 2

The aim of the current work is to apply the analysis tools developed in stage 1 to more complex models representative of real launch vehicles. Specifically, the current work is focussed on achieving the following objectives:

1. Extending the modal coupling modelling technique developed in stage 1 to a large composite cylinder that will be tested at Boeing. This system has many more modes in the frequency range of interest (compared to the small cylinder used in stage 1) and will

demonstrate the effectiveness of the modal coupling approach in analysing a realistic structure for which fully-coupled FEA is unsuitable.

2. Extending the modal coupling modelling to a Representative Small Launch Vehicle Fairing (RSLVF).

3. Developing a model of the fairing excitation field to determine the required loading parameters for the numerical model. A steady state free-field external pressure field excitation in the frequency range from 50Hz to 300Hz will be used as a first order approximation of the more complex launch environment.

4. Investigating the effectiveness of multi-degree-of-freedom devices in reducing sound transmission. This will involve multiple coupled elements making up a single device. The relative merits of such devices compared to simpler devices tuned to different frequencies will be evaluated.

5. Investigating passive absorber options for minimising interior noise levels in a launch vehicle excited with a realistic pressure field. This task presents new challenges because in the previous tasks, a volume occupied by the VAD was subtracted from the volume for the cavity, and then a modal analysis of the cavity was performed. In stage 1 it was assumed that the size and location of the VAD would not change which meant that the mode shapes of the cavity would not change.
   If the location of the VAD is to be optimised then the mode shape of the cavity will change slightly when the VAD is put in the new location. An approximation will be developed for the effect of VAD(s) location and size on the mode shapes of the cavity. A genetic algorithm will be used to optimise the locations of the VADs on the structure. The results achieved using reactive elements will be compared against an equivalent mass approach.

The following text describes the work achieved to date. It is primarily focussed on realising accurate numerical models of the two platforms under investigation (RSLVF and Boeing cylinder) as well as validating the analysis techniques that will be used to evaluate the performance of the noise control measures in the final stage of the project.

2 ANSYS composites implementation

The Representative Small Launch Vehicle Fairing (RSLVF) and Boeing cylinder experimental rigs are both made of composite materials. This has led to a considerable increase in model complexity over the model in stage 1 of the project[1] where only isotropic thin shells were considered. The ANSYS[2] finite element program allows the analysis of composite materials by using specialised layered elements.

2.1 Layup Definitions

The ANSYS SHELL99 linear layered structural shell element is an 8 node, 3D shell element with 6 DOF at each node. It allows the application of material properties by two methods,

1. layer thickness (with up to 250 Layers), orientation and individual material properties (which are generally orthotropic), or

2. the ABBD matrix method[3].

The ABBD matrix method is a more general form for defining composite material properties. It allows one to define the relationships between forces and moments to strains and curvature respectively (stiffness). These matrices are usually calculated automatically by the FE code given layer properties and orientations (method 1), but can be calculated directly by external programs if required.

2.2 Fluid Structure validation

The SHELL99 element in ANSYS contains mid-side nodes. The FLUID30 element, the acoustic element with a pressure DOF is only available without mid-side nodes.

There was concern as to whether the modal coupling via the fluid / structure interface would be calculated correctly with only the outer nodes of the structural elements connected to the fluid nodes. In order for the coupling to work, three conditions needed to be satisfied:

- the displacement (or velocity) at the coupled nodes needed to be equal. Achieved by default through the Fluid-Structure Interface flag.
- the areas associated with each of the coupled nodes should be representative of the actual interface condition. That is, the surface integral must use the correct nodal areas. This necessarily excludes the mid side nodes of the structural elements. It was found that this condition is satisfied by default since it is the acoustic elements which are used to calculate the effective nodal area for the surface integral (see below for more detailed discussion).
- the wavelength of the highest acoustic and structural mode must be considerably larger than the distance between nodes. This is automatically satisfied with the constraints already placed on the mesh density.

The material below confirms that the above criteria are satisfied and that the modal coupling is accurately calculated.

One concern was how ANSYS would calculate the area associated with each coupled node. This is a non-standard use of the program and is was necessary to validate the use of both ANSYS and the MATLAB based modal coupling technique with this combination of elements and with various external loading combinations.

2.2.1 Baseline model

The model chosen to validate the techniques was based on the Stage 1 report empty cylinder model[1]; namely a steel cylinder capped at one end with an aluminium plate, and at the other with a stiff wooden cap. Figure 3 shows a half view of the structural element mesh of the empty cylinder.

The parameter used to validate the results was the sum of the squared nodal pressure throughout the cavity. This is a good estimate of the acoustic potential energy and was used rather than the true acoustic potential energy (volume integral of the squared pressure) since it was directly available from ANSYS.

Calculations were performed for a 4 noded shell element (SHELL63) and an 8 noded shell element (with mid-side nodes, SHELL99). Since the use of the SHELL63 element for modal coupling had been previously validated[1], if the two element types gave the same results then it could be concluded that coupling with the SHELL99 elements is accurate. Both ANSYS and MATLAB were used to calculate the system response for three loading conditions; namely:

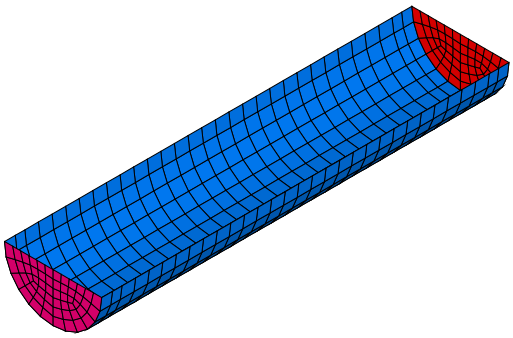

Figure 3: Baseline model geometry (stage 1 empty cylinder) - half view of structural elements only

- A single point force applied to the centre of the aluminium panel (see Figure 4),
- A unit pressure applied over the aluminium panel aimed at testing the frequency interpolation routine in the MATLAB code (see Figure 5), and
- Pressures calculated using COMET and applied over the whole body (see Figure 6).

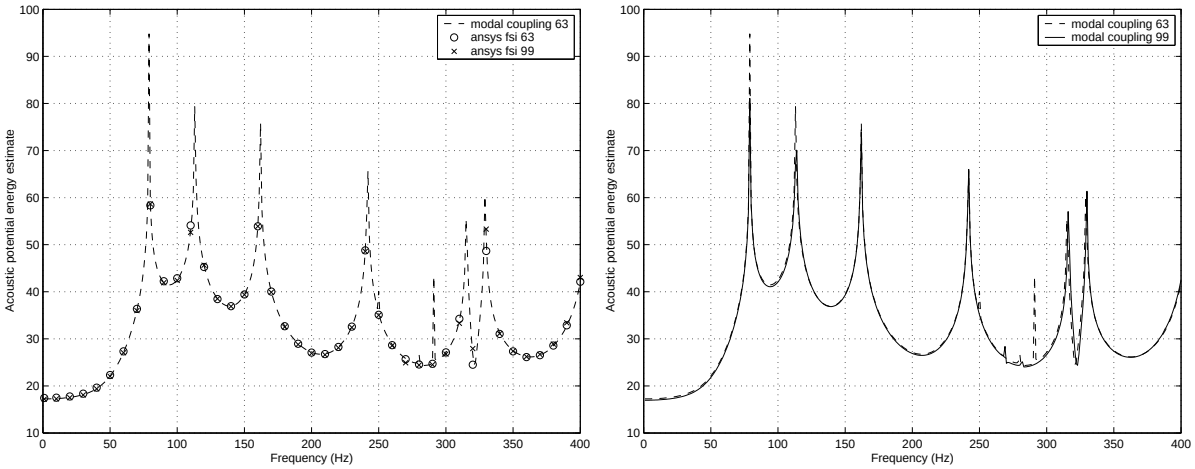

(a) Comparison between Ansys FSI with shell63 and shell99, and Matlab results (modal coupling) for shell63

(b) Comparison between Matlab results (modal coupling) for shell63 and shell99

Figure 4: Interior acoustic potential estimate for single point loading for stage 1 empty cylinder

Figures 4 to 6 show that the correlation between the SHELL63 and SHELL99 results is excellent. We can confidently use SHELL99 elements in modal coupling calculations. There is a slight discrepancy between the results using Shell63 and Shell99 near the resonance frequencies. This is simply due to the SHELL99 element being less stiff than the SHELL63 element and such behavior is expected from a quadratic element.

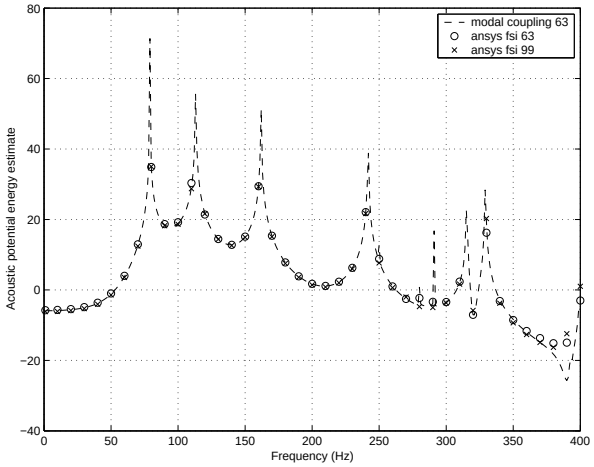

(a) Comparison between Ansys FSI with shell63 and shell99, and Matlab results (modal coupling) for shell63

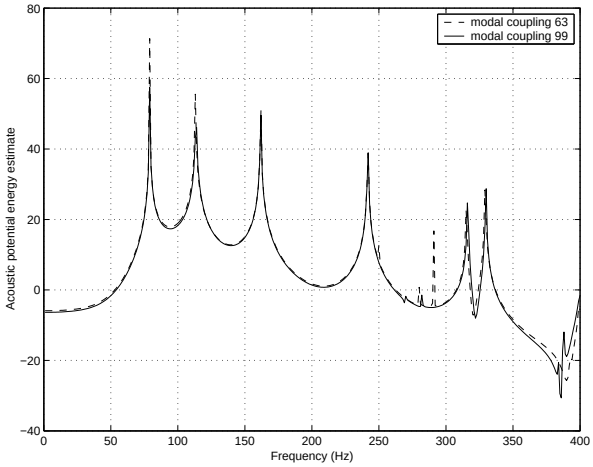

(b) Comparison between Matlab results (modal coupling) for shell63 and shell99

Figure 5: Interior acoustic potential estimate for unit pressure end loading for stage 1 empty cylinder

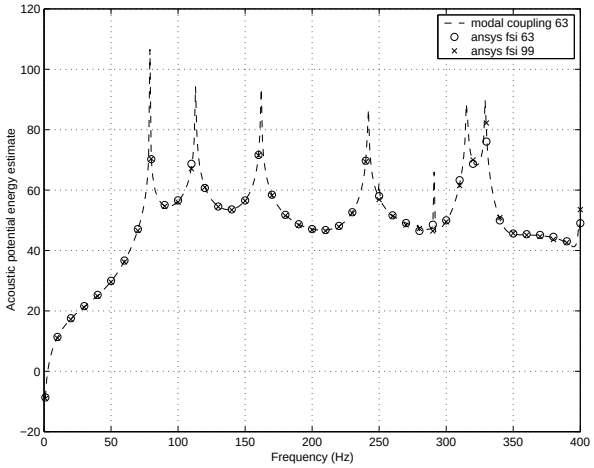

(a) Comparison between Ansys FSI with shell63 and shell99, and Matlab results (modal coupling) for shell63

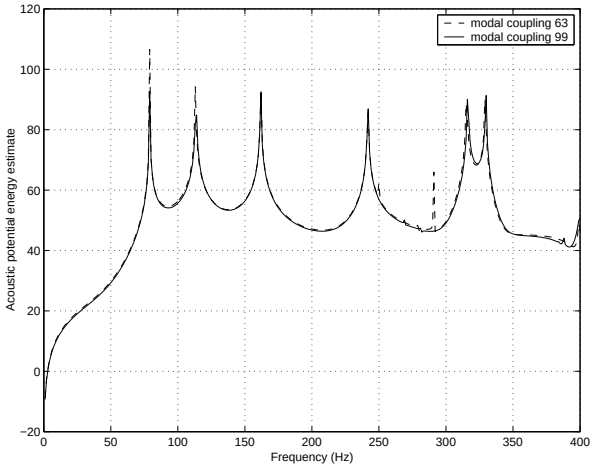

(b) Comparison between Matlab results (modal coupling) for shell63 and shell99

Figure 6: Interior acoustic potential estimate for COMET calculated pressure loading for stage 1 empty cylinder

3 Experimental / Numerical models

Structural FEA models of the RSLVF and the Boeing cylinder were available from AFOSR in the form of NASTRAN models. Unfortunately these models could not be utilised directly for two reasons;

- The University does not use NASTRAN but rather currently licenses and uses ANSYS,
- The modal coupling technique uses the results of separate structural and cavity acoustic modal analyses to analyse the coupled component. The current version of the code must have geometrically coincident nodes between the structural and acoustic models. The NASTRAN models only supplied the structural elements with no acoustic cavity.

3.1 Boeing cylinder

3.1.1 Physical Description

The cylinder is made of a composite layup, with wooden end-caps. The geometry of the device is shown in figure 7. The overall dimensions of the cylinder are reported in table 1.

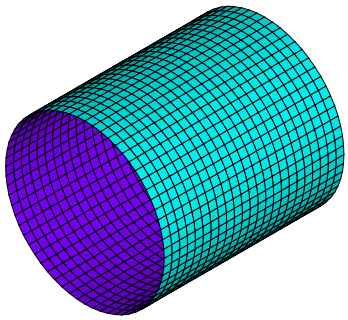

Figure 7: Boeing model geometry - view of structural elements only

Table 1: Boeing cylinder general properties

Property	Value
Cylinder Diameter	97" (2.46 m)
Cylinder Length	110" (2.79 m)
End cap thickness	5" (0.127 m)
Wood Young's modulus (E)	10e9 Pa
Wood density (ρ)	800 kg/m^3

3.1.2 Composite Definition

The layup is a 5 layer composite with 2 orthotropic materials. The layup specifications appear in Table 2. The weave and core material properties appear below in Table 3 and 4 respectively.

Table 2: Boeing cylinder layup specification

Layer	1	2	3	4	5
Property	weave	weave	core	weave	weave
Angle (degrees)	0	45	0	-45	0

Table 3: Boeing cylinder weave property

Property	Value
E_x	9e6 psi (0.621e11 Pa)
E_y	$= E_x$
E_z	$= E_x$
ν_{xy}	.045
ν_{yz}	$= \nu_{xy}$
ν_{xz}	$= \nu_{xy}$
G_{xy}	0.75e6 psi (0.517e10 Pa)
G_{yz}	$= G_{xy}$
G_{xz}	$= G_{xy}$
Density (ρ)	.000140 snails/inch^3 (1494 kg/m^3)
Thickness	0.0105" (0.27 mm)

3.1.3 FEA Models

The AFOSR NASTRAN model consisted of the composite cylindrical shell only. Stiff beams tied the edge of the shell to mass elements at the centre, and represented the effect of the end-caps. The first 4 non-rigid body natural frequencies of the shell, without the stiff beams & mass (i.e. a “free-free” end condition) were supplied as validation.

An ANSYS model was generated with end caps, and properties of the wood were assumed. This allows a contiguous model for the COMET calculations.

3.1.4 Comparison

For comparison with the NASTRAN models, the end-caps were ignored. The natural frequencies of the first 4 non-rigid body modes are listed in Table 5. The corresponding mode shapes appear in Figure 8.

Table 4: Boeing cylinder core property

Property	Value
E_x	100 psi (0.690e+6 Pa)
E_y	= E_x
E_z	= E_x
ν_{xy}	.01
ν_{yz}	= ν_{xy}
ν_{xz}	= ν_{xy}
G_{xy}	10 psi (0.690e+5 Pa)
G_{yz}	20000 psi (0.138e+9 Pa)
G_{xz}	14000 psi (0.965e+8 Pa)
Density (ρ)	.0000105 snails/inch^3 (112 kg/m^3)
Thickness	0.1875" (4.76 mm)

Table 5: Boeing cylinder natural frequency comparison (Hz)

Mode	NASTRAN	ANSYS
7	3.8587	3.7760
8	3.8587	3.7760
9	4.6588	4.6272
10	4.6588	4.6272

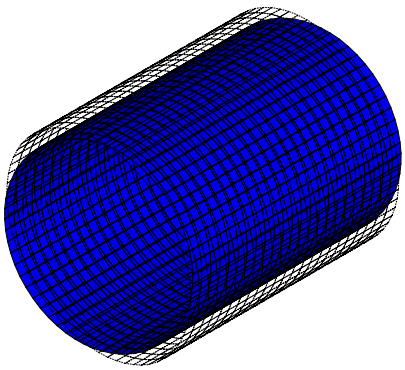

(a) Mode Shape 7

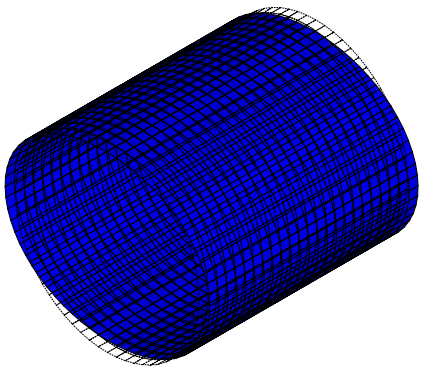

(b) Mode Shape 8

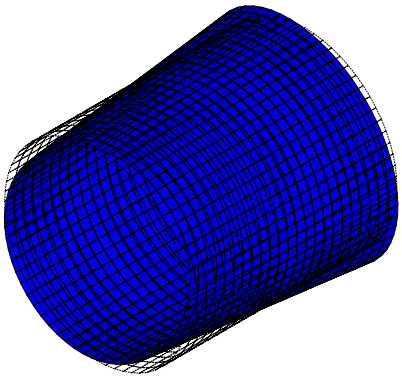

(c) Mode Shape 9

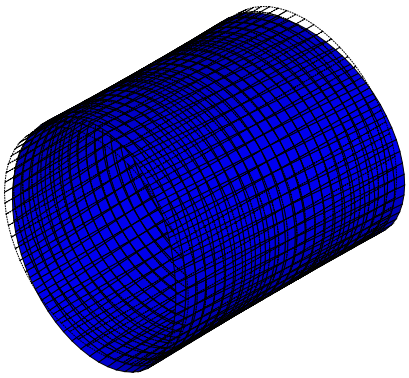

(d) Mode Shape 10

Figure 8: Boeing cylinder mode shapes

The extremely good correlation between the NASTRAN and ANSYS results indicates the composite properties have been entered correctly and that the ANSYS model can be used with confidence for further study.

3.2 Representative small launch vehicle fairing (RSLVF)

3.2.1 Physical Description

The RSLVF 9 is an axi-symmetric launch vehicle, made of composite material, that could be considered typical for small launch vehicles. The overall dimensions of the vehicle are reported in Table 6.

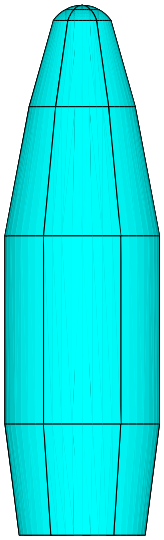

Figure 9: RSLVF geometry

Table 6: RSLVF general properties

Property	Value
Maximum Diameter	1.552 m
Overall Length	5.33 m

3.2.2 Composite Definition

The properties of the RSLVF were supplied in ABBD matrix form, rather than as a composite layup. The reason for this was that the RSLVF has “ribs”, and the ABBD matrix method allows the effect of these ribs to be included in the material properties, rather than explicitly modelling them and increasing solution time. The ABBD matrix properties are given in Table 7. Since the properties were supplied in 3x3 matrix form, which is appropriate for thin shells, they were converted to a more general 6x6 format as used by ANSYS, according to Equation 14.99 of the ANSYS theory manual[4].

Table 7: RSLVF ABBD matrix properties

Property	Value (N/m^2)	Property	Value (N/m)	Property	Value (N)
A_{11}	1.4008e+008	B_{11}	277760	D_{11}	5.3840e+003
A_{12}	2.4660e+007	B_{12}	62880	D_{12}	1.0360e+003
A_{13}	0	B_{13}	0	D_{13}	0
A_{22}	7.7720e+007	B_{22}	604800	D_{22}	5.9427e+003
A_{23}	0	B_{23}	0	D_{23}	0
A_{33}	2.5020e+007	B_{33}	66200	D_{33}	1.0747e+003

3.2.3 FEA Models

Two RSLVF models were analysed resulting in the two different meshes as illustrated in Figure 10. The “old” model uses the element definition of the NASTRAN model imported directly into ANSYS. The “new” model uses a quad dominant mesh directly generated in ANSYS. This model also generates the cavity mesh for the acoustic modes at the same time as the structural mesh, and hence has coincident nodes.

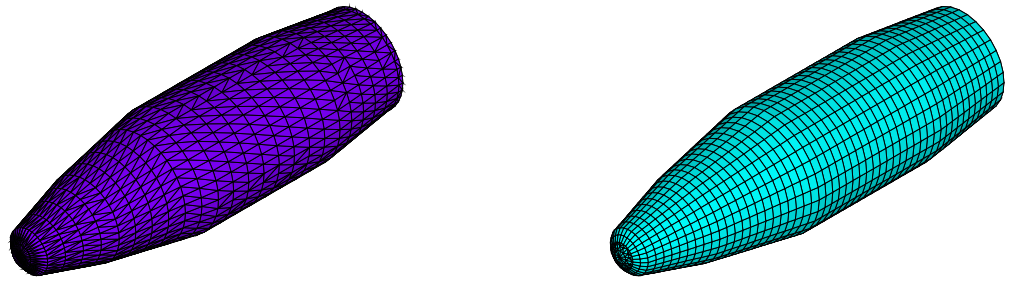

(a) Old Mesh (b) New Mesh

Figure 10: RSLVF mesh

3.2.4 Comparison

The natural frequencies of the first 14 modes are listed in table 8. The first 10 mode shapes appear in Appendix A, Figures 11 to 20. The extremely good correlation between the NASTRAN and ANSYS results indicate the composite properties have been entered correctly and that the ANSYS model can be used with confidence for further study.

Table 8: RSLVF natural frequency comparison (Hz)

Mode	NASTRAN	ANSYS(old)	Difference (old)	ANSYS (new)	Difference (old)
1	49.00	47.56	-3%	48.70	-1%
2	49.16	47.56	-3%	48.70	-1%
3	102.72	98.79	-4%	100.95	-2%
4	103.73	98.80	-5%	100.95	-3%
5	120.99	118.71	-2%	120.55	0%
6	122.98	118.77	-4%	120.55	-2%
7	170.33	165.85	-3%	169.09	-1%
8	178.42	180.02	1%	177.33	-1%
9	179.48	180.14	0%	177.33	-1%
10	181.46	180.86	0%	186.07	3%
11	188.29	180.89	-4%	186.07	-1%
12	194.29	181.30	-7%	188.54	-3%
13	194.87	181.37	-7%	188.54	-3%
14	206.81	202.48	-2%	205.34	-1%

4 Conclusions

The work to date has shown that the ANSYS Finite Element models of the two launch vehicles are accurate. It has also been shown that the modal coupling technique with its associated faster computing time produces accurate estimates of the interior sound field when compared against that predicted using a fully coupled FE model. The more efficient modal coupling technique can now be used in the absorber optimisation procedure, which is the last objective discussed in the introduction. Prior to doing this work, the third and fourth objective will be addressed.

References

[1] C.H. Hansen, A.C. Zander, B.C. Cazzolato, and R.C. Morgans. Investigation of passive control devices for potential application to a launch vehicle structure to reduce the interior noise levels during launch. Final report for stage 1, The University of Adelaide, 2000.
[2] ANSYS Theory Manual. *Ansys 5.4*. Ansys Inc, Canonsburg, PA, 8 edition, 1998.
[3] F.L. Matthews and R.D. Rawlings. *Composite materials: engineering and science*. Chapman and Hall, 1994.
[4] ANSYS Theory Manual. *Ansys 5.6*. Ansys Inc, Canonsburg, PA, 8 edition, 2000.

A RSLVF Mode shapes.

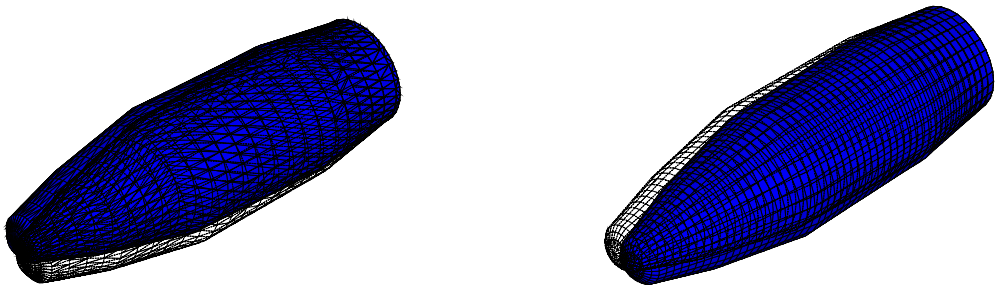

(a) Old Isometric (b) New Isometric

(c) Old Side (d) New Side

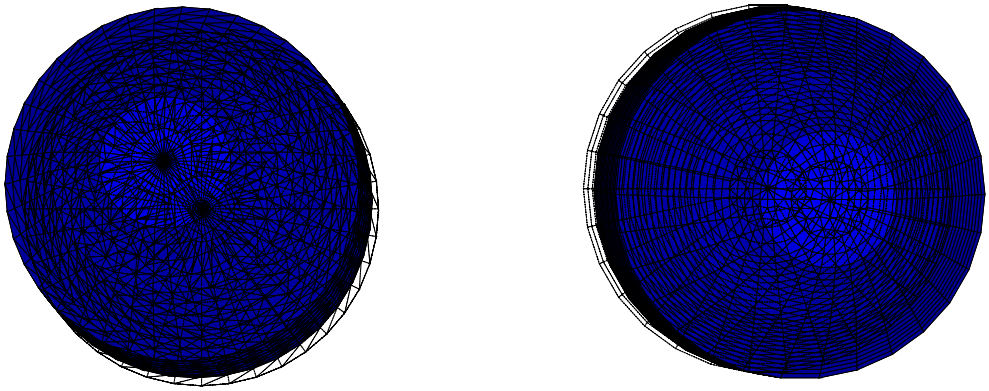

(e) Old End (f) New End

Figure 11: RSLVF mode shape 1

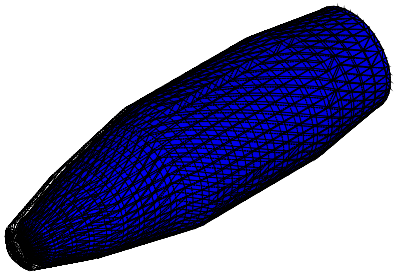

(a) Old Isometric

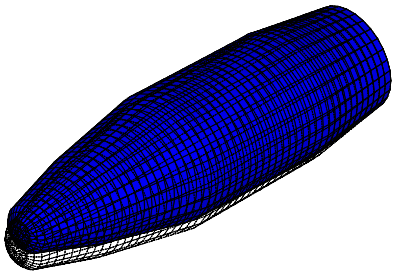

(b) New Isometric

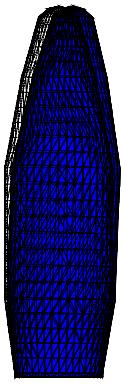

(c) Old Side

(d) New Side

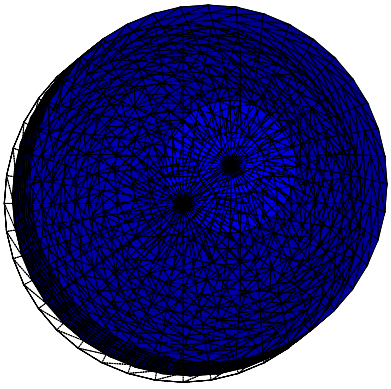

(e) Old End

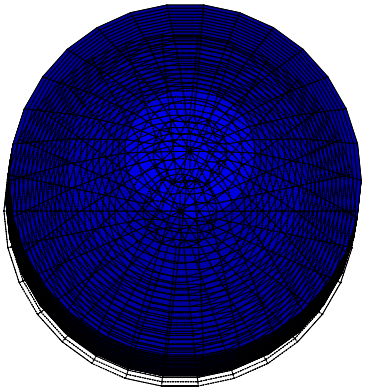

(f) New End

Figure 12: RSLVF mode shape 2

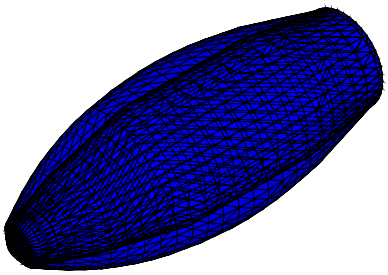

(a) Old Isometric

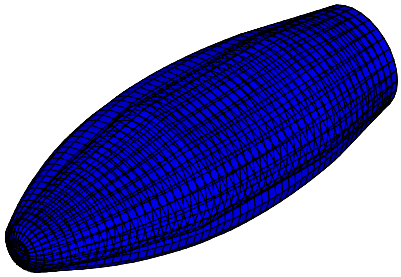

(b) New Isometric

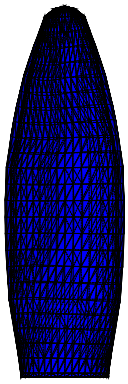

(c) Old Side

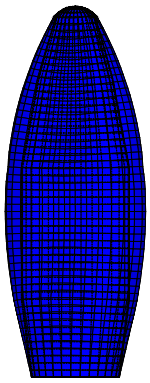

(d) New Side

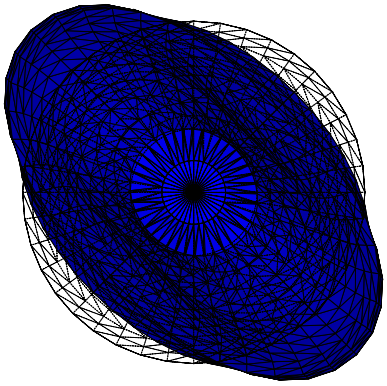

(e) Old End

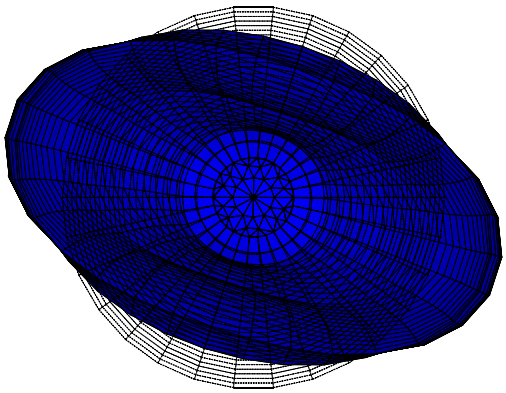

(f) New End

Figure 13: RSLVF mode shape 3

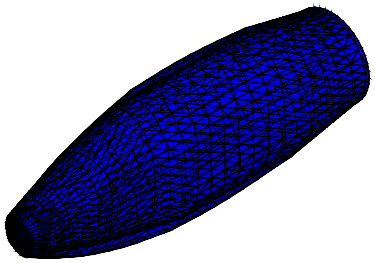

(a) Old Isometric

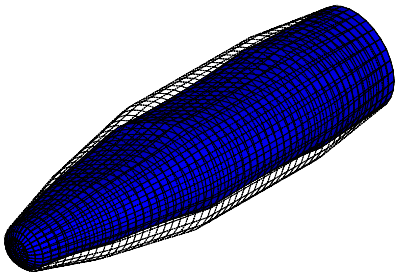

(b) New Isometric

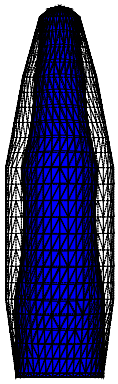

(c) Old Side

(d) New Side

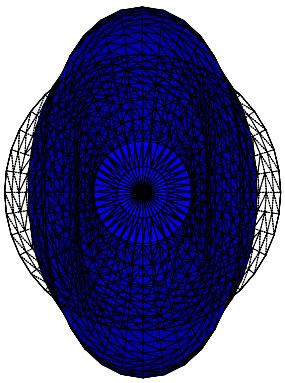

(e) Old End

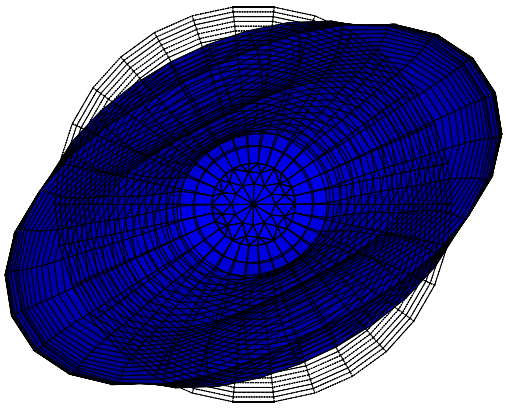

(f) New End

Figure 14: RSLVF mode shape 4

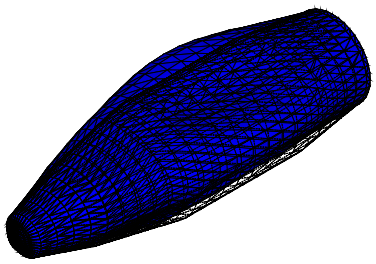

(a) Old Isometric

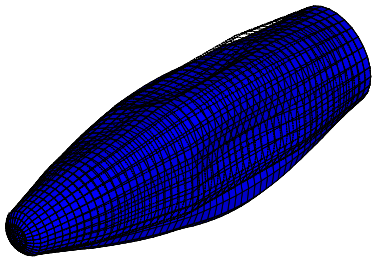

(b) New Isometric

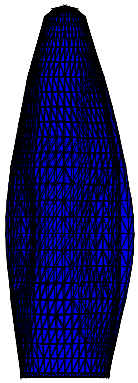

(c) Old Side

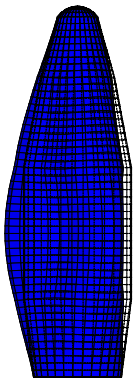

(d) New Side

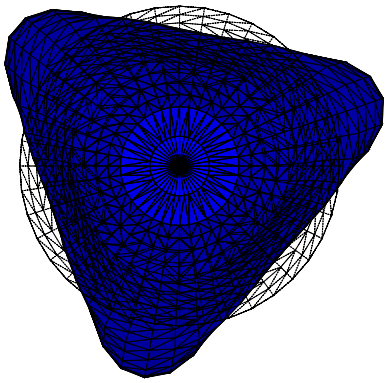

(e) Old End

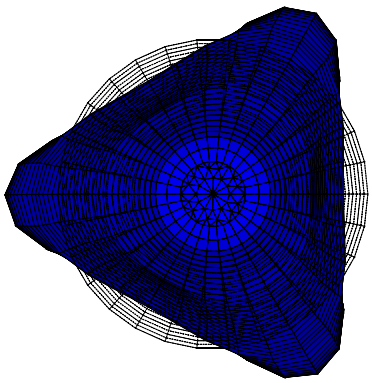

(f) New End

Figure 15: RSLVF mode shape 5

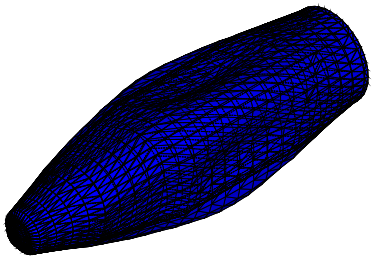

(a) Old Isometric

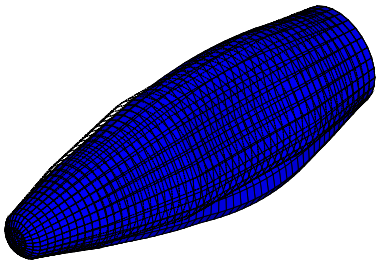

(b) New Isometric

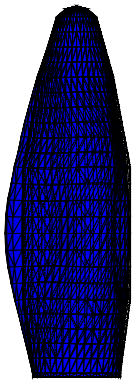

(c) Old Side

(d) New Side

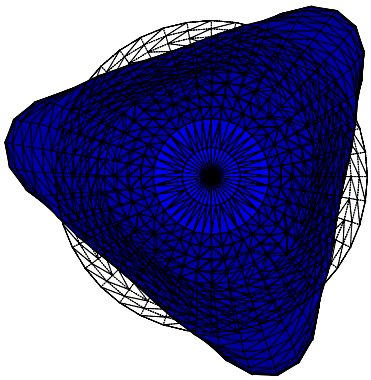

(e) Old End

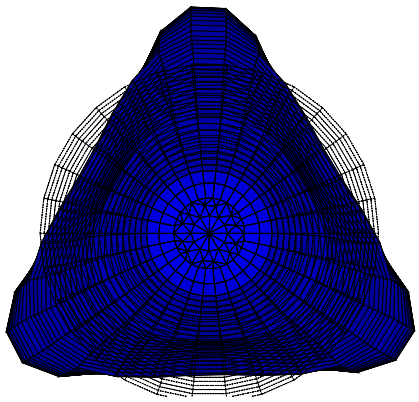

(f) New End

Figure 16: RSLVF mode shape 6

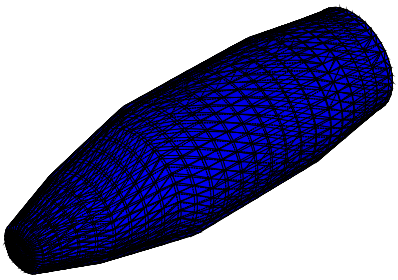

(a) Old Isometric

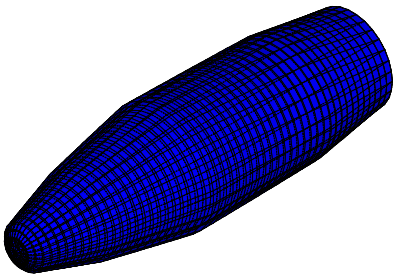

(b) New Isometric

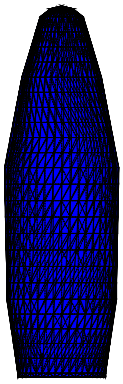

(c) Old Side

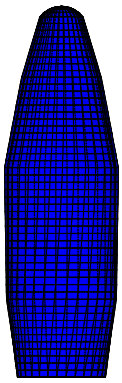

(d) New Side

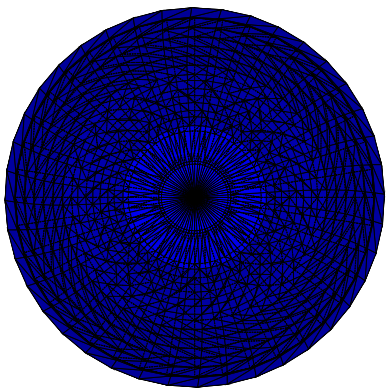

(e) Old End

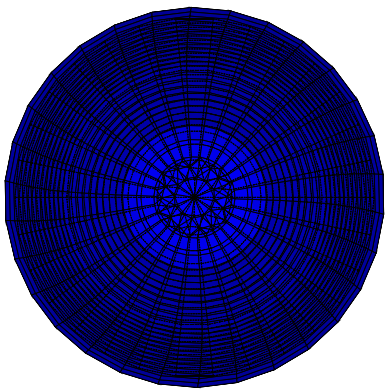

(f) New End

Figure 17: RSLVF mode shape 7

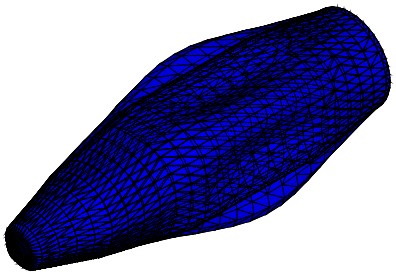

(a) Old Isometric

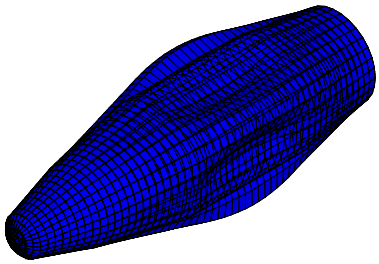

(b) New Isometric

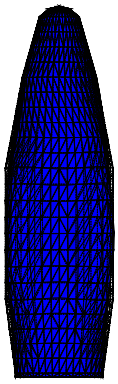

(c) Old Side

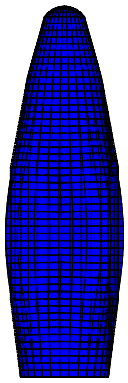

(d) New Side

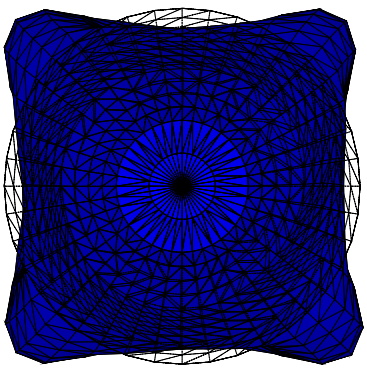

(e) Old End

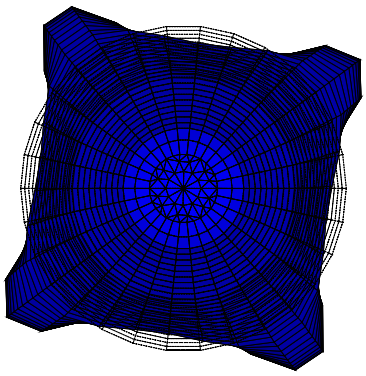

(f) New End

Figure 18: RSLVF mode shape 8

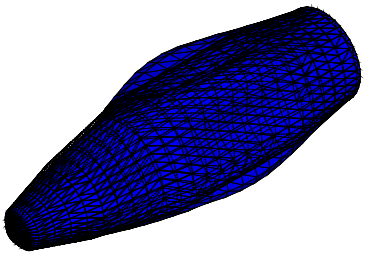

(a) Old Isometric

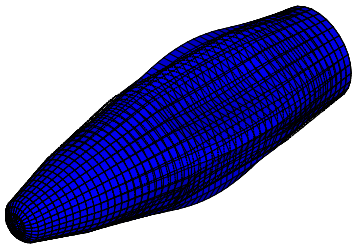

(b) New Isometric

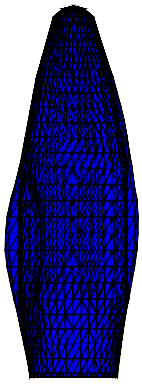

(c) Old Side

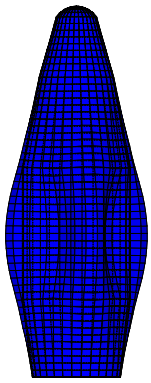

(d) New Side

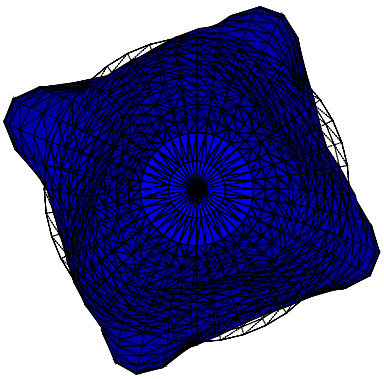

(e) Old End

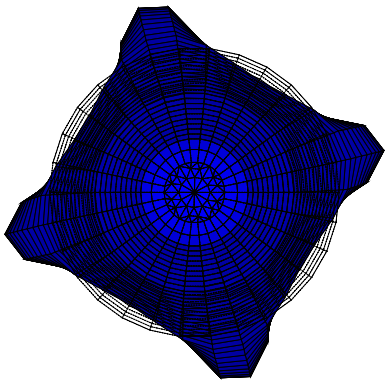

(f) New End

Figure 19: RSLVF mode shape 9

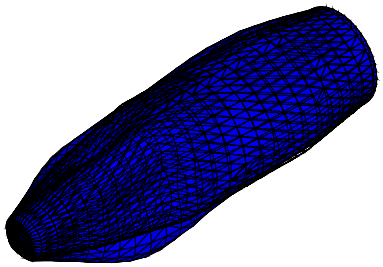

(a) Old Isometric

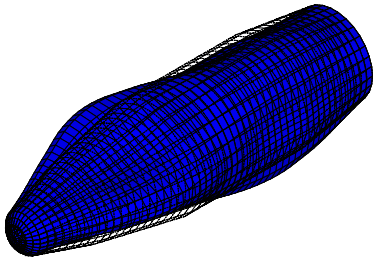

(b) New Isometric

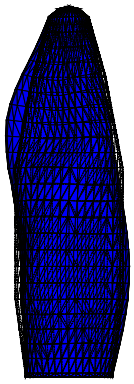

(c) Old Side

(d) New Side

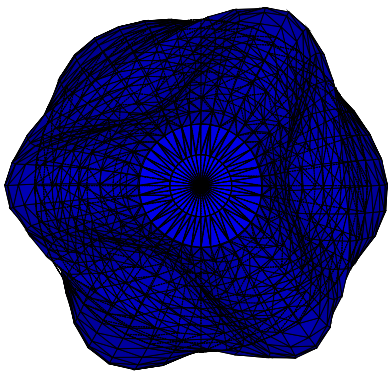

(e) Old End

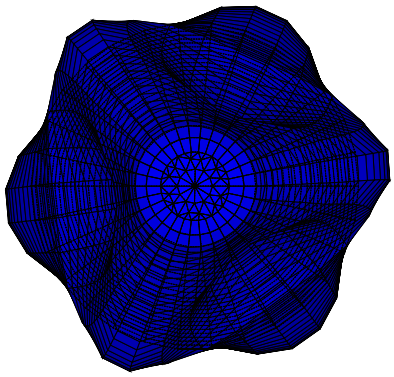

(f) New End

Figure 20: RSLVF mode shape 10